

Different configurations of transferred atmospheric pressure plasma jet and their application to polymer treatment

Fellype do Nascimento, Konstantin Kostov

São Paulo State University - UNESP, Guaratinguetá, Brazil

Antje Quade

Leibniz Institute for Plasma Science and Technology - INP, Greifswald, Germany

Mara Adriana Canesqui

State University of Campinas - UNICAMP, Campinas, Brazil

May 10, 2022

Abstract

The employment of atmospheric pressure plasma jets (APPJs) in a large sort of applications is limited by the adversities related to the size of the treated area and the difficulty to reach the target. The use of devices that employ long tubes in their structure has contributed significantly to overcome these challenges. In this work, a comparison between two different plasma systems employing the jet transfer technique is presented. The main difference between the two devices is how the long plastic tube was assembled. The first one uses a copper wire placed inside a long plastic tube. The other device has a metallic mesh installed in a concentric arrangement between two coaxial plastic tubes. As a result, the two APPJ systems exhibit different properties, with the wire assembly being more powerful, also presenting higher values for the electrical current and rotational temperature when compared to the mesh mounting. X-ray photoelectron spectroscopy (XPS) demonstrates that both configurations were capable of inserting O-containing functional groups on the polypropylene (PP) surface. However, the transferred plasma jet with wire assembly was able to add more functional groups on the PP surface. The results from XPS analysis were corroborated with water contact angle measurements (WCA), being that lower WCA values were obtained when the PP surface presented higher amounts of O-containing groups. Surface morphology evaluation showed that the plasma treatment tends to slightly increase the surface roughness of the PP samples with both wire and mesh configurations. Furthermore, the findings in this work suggest that the APPJ with wire configuration is more appropriate for material treatments, while the transferred jet with mesh arrangement tends to present lower electrical current values which makes it more suitable for biological applications.

Keywords: *DBD plasma; plasma jets; plasma properties; transferred plasma; plasma treatment; polymer treatment*

1 Introduction

In recent years atmospheric pressure plasma jets (APPJs) produced in open environment have received a lot of attention, not only because of their versatility and ease of use, but also due to the

encouraging results achieved in the most diverse applications [1, 2, 3, 4]. Special attention has been given to medical and biological applications of APPJs, whose beneficial effects have been attributed to the reactive oxygen and nitrogen species (RONS) produced by the plasma jets [5, 6, 7]. The actions of the RONS are not only limited to biological materials, since they also contribute to the hydrophilization and surface activation processes of a large number of materials treated with APPJs [8, 9].

Most APPJ devices produce plasma jets with small cross-section area, ranging from a several square millimeters to few square centimeters (usually less than 2 cm^2). In most cases this is a limitation, since the targets to be treated with APPJs usually have larger dimensions. In other cases, like in dentistry and medicine, it is an advantage because it provides a localized treatment. However, in all situations, it is necessary to provide a way for the plasma to reach the target to be treated. Whether it is bringing the target closer to the device that produces the plasma, or finding a way to bring the plasma to it. For the last purpose, some devices that produce plasma jets at the end tip of long and flexible tubes have been developed [6, 10, 11, 12, 13, 14, 15, 16, 17, 18, 19, 20, 21, 22, 23, 24, 25]. Being that some of them use the plasma jet transfer technique, which is basically a secondary plasma jet formed away from a primary discharge that is generated inside a reactor or from a primary plasma jet [6, 15, 17, 24, 26, 27]. One of the advantages of use the jet transfer technique in APPJ devices with long tubes is that the plasma jet is produced far from the high voltage source which improves the electrical safety in its operation and handling. Furthermore, the use of the jet transfer technique facilitates the employment of an APPJ to treat large target materials by scanning their surfaces.

One of the problems related to the generation of plasma jets using long polymeric tubes is the possibility of plasma production in the tube length instead of obtaining a plasma jet only at the end tip of the tube. This is a problem because the plasma tends to interact with the tube material causing a degradation. Some studies found that this can be prevented by using a second tube surrounding the first, with a space to flow a different gas between the two tubes [21, 28]. A study by Onyshchenko *et al* aimed to investigate penetration depth of plasma inside flexible tubes suggests that this problem can be minimized by employing long tubes with an appropriated internal diameter [29]. In that work it was observed that the plasma penetration depth in tubes depends on their internal diameters, being that there is a certain tube diameter that maximizes the penetration depth.

The devices that employ long and flexible tubes to produce plasma jets for materials treatment have shown results that are as good as those that do not use long tubes. However, the most interesting results are related to the possibility of performing treatments in cavities, specially in combination with endoscopes [21, 22, 28]. Nonetheless, before to apply a new configuration or technique to produce APPJ on biological materials or on *in vivo* targets, it is convenient, and also a common practice, to begin studies with inorganic materials like polymers.

In this work we present a modified design concept using the jet transfer to generate APPJs at the ends of long and flexible tubes. It consists of a metallic mesh placed between two long plastic tubes in a concentric arrangement. The main objective of using this design is to reduce the electrical current that flows through the plasma jet thus making it more suitable for *in vivo* applications. This configuration was compared with another that employs a metal wire inside a long tube. Both devices were characterized with electrical and optical diagnostics and comparisons of the plasma parameters obtained on each case are provided. A study comparing the use of the two different configurations for polymer treatment was also performed. The results revealed differences in the

surface treatments when each configuration is used.

2 Experimental setup

Figure 1(a) shows the experimental setup used in this work, with a detailed view of the two long tube configurations illustrated in Fig. 1(b). The plasma jet device presented in Fig. 1 is based on a DBD type reactor, composed by a metal pin electrode encapsulated in a closed-end quartz tube, which in turn is placed inside a dielectric chamber. Completing the device, there is a 1-meter long and flexible plastic tube connected to the DBD reactor. In this work, the long tube employed to produce APPJ was assembled in two different ways. In the first one a 0.5 mm thin copper wire is put inside a plastic tube, whose material is Nylon 6, with outer diameter (OD) equals to 4 mm and inner diameter (ID) equals to 2 mm. In the second configuration the long tube is composed by a metallic mesh, with 90% closed area extended over a polytetrafluoroethylene (PTFE) tube with OD = 3 mm and ID = 2 mm, being that both of which are placed inside a Nylon 6 tube with OD = 6 mm and ID = 4 mm.

Both the wire and the mesh are fixed to a metallic connector that goes inside the reactor and acts as a floating electrode (see Fig. 1). Besides that, each set formed by the long tube and metallic connector is attached to its own exchangeable coupler, which is made of polyoxymethylene (POM). Furthermore, both copper wire and metallic mesh ends 2 mm before the plasma outlet, and in the last configuration there is an electrical insulation at the end of the mesh in order to avoid discharges coming directly from it.

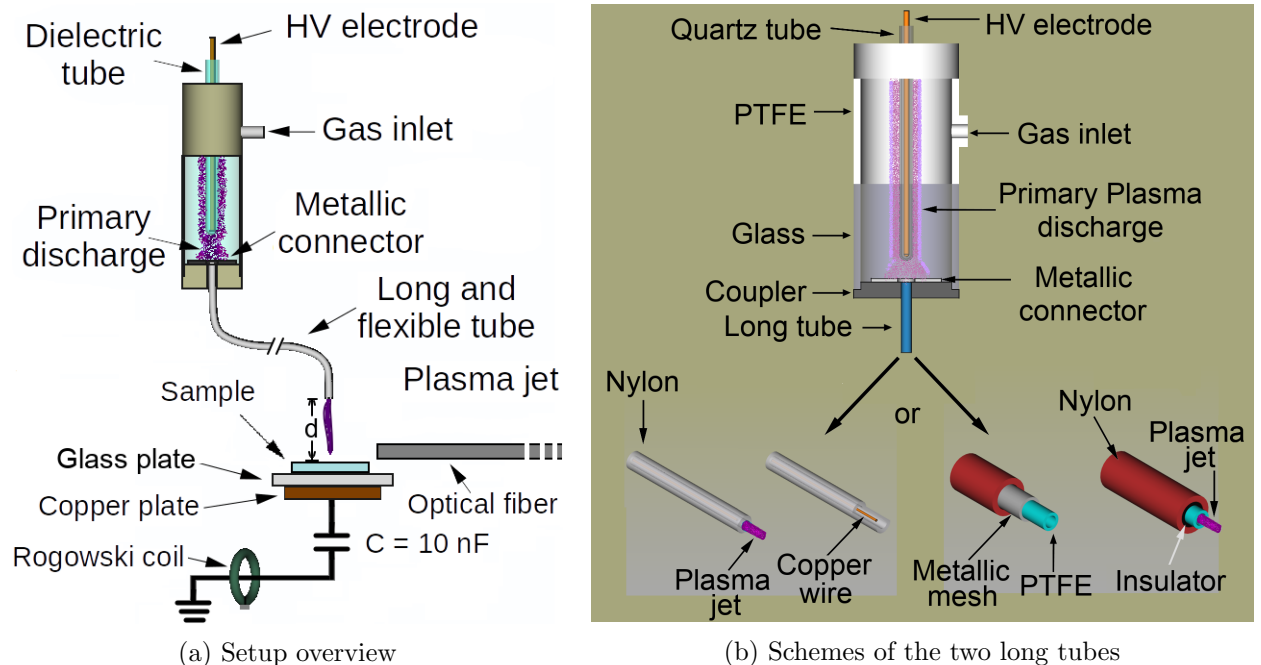


Figure 1: (a) Overview of the experimental setup. (b) Details of the two long tube configurations.

In order to produce plasma the working gas, argon (Ar) for instance, is fed into the chamber and flows through the long and flexible plastic tube connected to the reactor. At the same time a

high voltage (HV) signal is applied to the HV electrode and a primary discharge is formed inside the reactor chamber. When the primary discharge is on, it polarizes the metallic connector, which is linked to the copper wire or metallic mesh, and a small plasma jet is ignited at the distal end of the plastic tube. The remote plasma jet produced in each case was directed at normal incidence towards a target, placed at a distance $\mathbf{d} = 6$ mm from the plasma outlet. We performed the electrical and optical characterizations using two different targets. One of them was a dielectric material (the glass plate in Fig. 1(a)) lying over a grounded copper plate. And the other was the copper plate itself.

The power source employed to produce the plasma jets was a commercial AC generator from GBS Elektronik GmbH (model Minipuls4). We choose to apply a HV waveform that resembles a sinusoidal “burst” instead of a pure sinusoidal signal because the former produces lower ohmic heating on the DBD reactor and on other parts of the device. The oscillation frequency (f_{osc}) in the burst HV was 27 kHz. This f_{osc} value was chosen as the one that produce the most stable plasma jets in both wire and mesh configurations. The HV burst is followed by a voltage off period, which repeats at a repetition period (τ) of 1.7 ms. An example of the typical HV waveform applied to the powered electrode is depicted in Fig. 2.

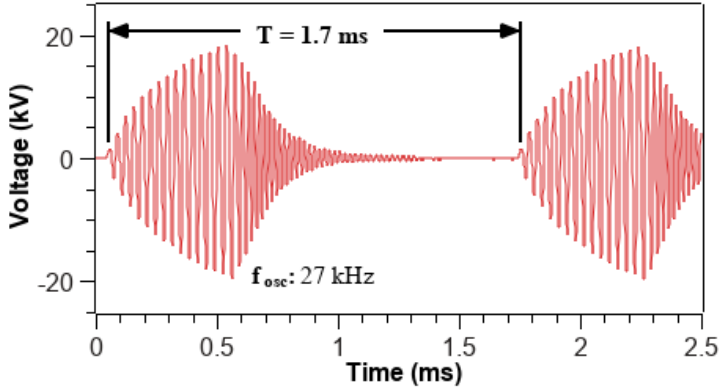


Figure 2: Example of a typical HV waveform applied to the pin electrode without producing plasma.

Simultaneous measurements of the voltage applied on the powered electrode and the voltage across a serial capacitor ($C = 10$ nF) were carried out in order to obtain the average discharge power (P_{dis}). The calculation of P_{dis} values takes into account all voltage oscillations in each burst that produce a charge variation in C . The applied voltage was measured using a 1000:1 voltage probe (Tektronix, model P6015A) and the waveforms were recorded using a 200 MHz oscilloscope (Tektronix, model 2024B). Then, the P_{dis} value is calculated by summing the area of the $q - V$ Lissajous figures formed between the voltage ($V(t)$) and charge ($q(t)$) signals, divided by the burst period τ , that is [30, 31, 32]:

$$P_{dis} = \frac{1}{\tau} \oint q(V)dV \quad (1)$$

By applying the Green’s theorem to (1), P_{dis} can be calculated using:

$$P_{dis} = \frac{1}{2\tau} \int_{t_1}^{t_2} [V(t)q'(t) - V'(t)q(t)] dt \quad (2)$$

where $\{V'(t), q'(t)\} = d\{V(t), q(t)\}/dt$. An advantage of using Eq.(2) to calculate the area of the Lissajous figure is that it can be done without the need to plot the $q - V$ curve.

We also measured the waveform of the current that passes through the system using a Rogowski coil from PearsonTM (model 4100), which was used to obtain the effective discharge current (i_{RMS}).

To observe the light emission from multiple excited species and evaluate the production of the OH and NO species in the plasma, a broad-band optical emission spectroscopy (OES) in the wavelength range from 200 nm to 750 nm was performed using a multi-channel spectrometer from Avantes (model AvaSpec-ULS2048X64T), with spectral resolution (FWHM) equal to 0.76 nm. The light emitted by the plasma jet was collected using an optical fiber placed close to the surface target. The distance between the center of the plasma column and the fiber optic light input was 5 mm.

Spectroscopic measurements were also used to obtain rotational and vibrational temperatures (T_{rot} and T_{vib} , respectively) of N₂ molecules. In order to obtain T_{rot} and T_{vib} values, we used spectral emissions from the N₂ second positive system, $C^3\Pi_u, \nu' \rightarrow B^3\Pi_g, \nu''$, with $\Delta\nu = \nu' - \nu'' = -2$, in the wavelength range from 362 to 382 nm [33, 34, 35, 36]. Spectra simulations were carried out using the massiveOES software [37, 38]. Thus, comparisons between measured and simulated spectra were performed and the temperature values that generate a simulated curve that best fit to the experimental spectrum are chosen as the T_{rot} and T_{vib} values of the plasma jet. It is known that spectroscopic measurements performed with low-resolution spectrometers, like the Avantes one, are not sufficient to fully resolve the rotational levels of the N₂ molecules, which is a requirement to obtain accurate values for the T_{rot} parameter. However, there is a direct relationship between the shape and broadening of the N₂ vibrational bands and the variation of the T_{rot} values, being that the higher the T_{rot} , the larger the broadening and also the higher the intensity of the rotational lines in the vibrational bands. Both effects cause a change in the shape of the vibrational bands in that part that degrades to violet, causing it to become higher and wider, allowing the estimation of the T_{rot} values by using low-resolution spectrometers. Thus, even not very accurate, the T_{rot} values measured with the Avantes spectrometer can be good enough to show the trend of that parameter in the experiments performed in this work.

In this work we chose to perform the spectroscopic measurements in close proximity to the target surface because this is the portion of plasma that enters in contact with the material under treatment. So, this seems to be the most appropriate measurement for possible observations of the effects of the target's material on the plasma jets. However, when performing such measurements close to the surface of the target and using the data to measure the rotational temperatures, the T_{rot} values obtained may be different from the T_{gas} ones [34].

The APPJs produced with both wire and mesh configurations were also applied on polypropylene (PP) samples as a way to evaluate the effects of the plasma properties on the treatment of materials. Those effects were analyzed mainly by measurements of water contact angle (WCA), X-ray photoelectron spectroscopy (XPS) and morphology studies. The XPS measurements were performed with an equipment from Kratos (model Axis Supra), whose energy resolution is better than 1 eV on polymers and the local resolution is better than 15 μm . WCA measurements were carried out with a goniometer from Ramé-Hart (model 300), using the sessile drop method. Surface morphology analysis were performed using an optical profiler from Nanovea (model PS50).

The PP samples used in this work are commercially available materials and present high density

values. All the samples used have 1-mm thickness and approximately the same dimensions (35 mm x 25 mm).

3 Results and discussion

3.1 Discharge electrical parameters for the different configurations

In Fig. 3 are shown the typical voltage and current waveforms measured using a metallic (copper) target (a) and a dielectric (glass) one(b) for both wire and mesh configurations. It can be observed in the condition that the APPJ impinges the copper target, that when we switch from wire to mesh configurations there is an increase in the peak value of the applied voltage. However, what we have in fact is that the use of the wire configuration to produce the APPJ causes a voltage drop on the applied voltage, since the power source is configured to deliver always the same energy to the APPJ device, independently of the configuration in use. In other words, the peak voltage value is always the same (~ 15 kV-peak) when there is no plasma discharge in both configurations, and it looks like the waveform shown in Fig. 2. By keeping the nominal voltage constant instead of adjusting the actual applied voltage to the same value in all cases, we intend to evaluate the effect of the configuration (wire or mesh) on the electrical parameters of the plasma jet as a whole, since we are also dealing with different geometries of the conductor inside the long tube. Furthermore, that voltage drop is strongly linked to the higher electrical current values obtained in the wire configuration. Nevertheless, the magnitude of the voltage drop obtained with the wire configuration is much lower when we use the glass plate as the target, which confirms the latest statement. In addition, with the glass target there is no significant differences in the voltage drop when we switch the configuration from wire to mesh.

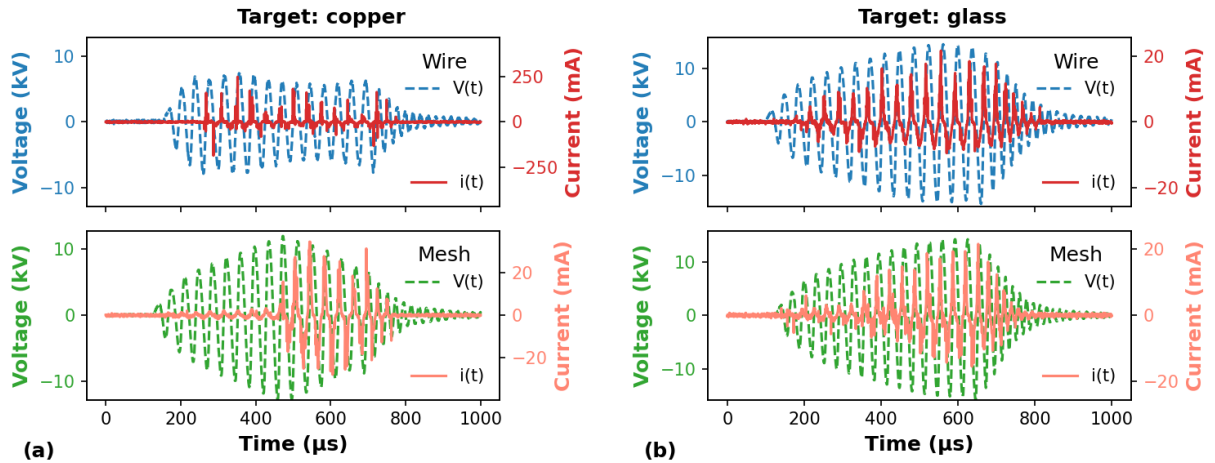


Figure 3: Typical waveforms of applied voltage ($V(t)$) and discharge current ($i(t)$) using (a) copper and (b) glass as targets, for both wire and mesh configurations. The gas flow rate was 2.0 l/min in all cases.

Figure 3 also shows that there is a clear delayed ignition in the plasma discharge and a shorter discharge duration when the mesh is used in comparison with the wire configuration. Such delayed

discharge is less evident when the glass target is used. Regarding the amplitude of current signals shown in Fig.3, it can be seen that when the plasma jet impinges the copper target the peak values are much higher (by one magnitude order) in the wire configuration than in the mesh one. However, the amplitude of the current signals are of the same magnitude order when the plasma jet impinges the glass target.

The discharge power (P_{dis}) and the electrical current, presented in this work as the root mean square value of the current waveform (i_{RMS}), are the most important electrical parameters in APPJs. Usually, it is desirable to have APPJs with adequate power values and low electrical current. Being that the last condition is highly desired for *in vivo* applications. However, plasma jets with low P_{dis} values are also useful when sensitive materials are under APPJ treatment.

Figure 4 shows the curves of P_{dis} and i_{RMS} as a function of the gas flow rate (Q) for a fixed distance ($d = 6$ mm) between the plasma outlet and the target. The results obtained for the metallic and the dielectric targets are shown in Figs. 4(a) and 4(b), respectively. For both targets the curves of P_{dis} and i_{RMS} vs Q were measured for the two 1-meter long tube configurations studied in this work. The first noticeable difference when we compare the wire and the mesh configurations is that the P_{dis} curves present higher values in the wire configuration. Considering the employment of the copper target, the two P_{dis} curves present similar trends, decreasing as the gas flow rate increases, being that the P_{dis} values obtained with the wire are, in general, $\sim 60\%$ higher than those obtained with the mesh. On the other hand, the i_{RMS} curves present different behaviors. When the wire is used, the i_{RMS} curve has a nearly parabolic shape with a peak value at $Q \approx 1.5$ l/min, while the i_{RMS} values are almost constant when using the mesh configuration. Also, the average i_{RMS} values are nearly three times higher when the wire is employed.

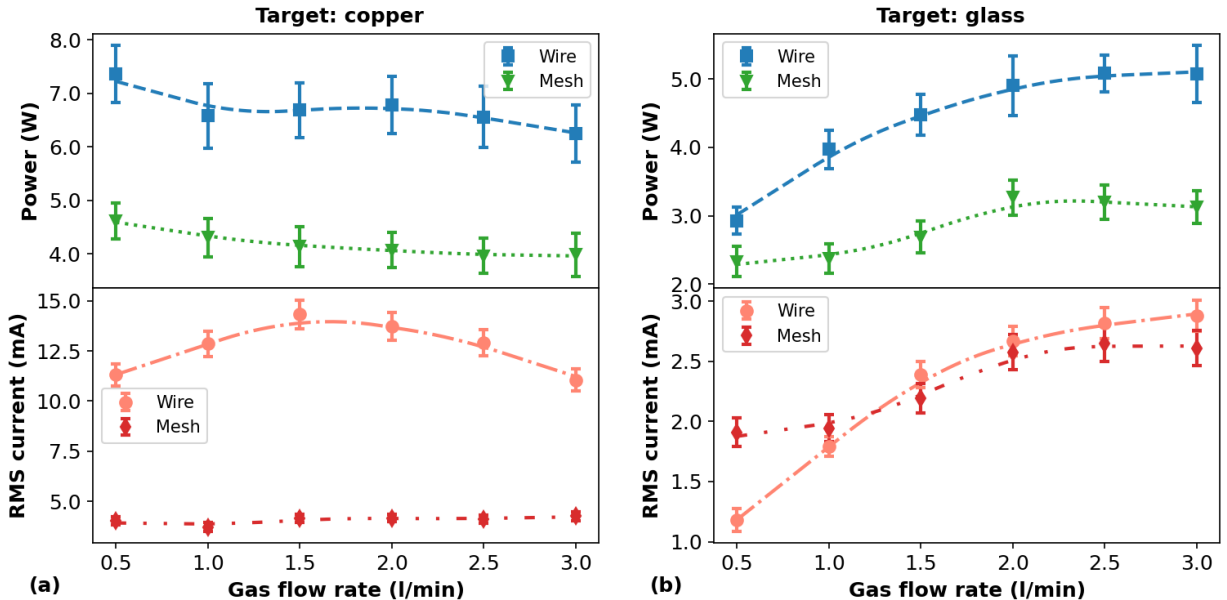


Figure 4: Discharge power and effective current as a function of the gas flow rate using (a) copper and (b) glass as target.

The explanation for the lower values of P_{dis} and i_{RMS} obtained with the mesh configuration when compared to the wire one is quite simple: the PTFE tube inside the mesh electrode acts as an additional dielectric barrier. So, this can be used as a way to improve the electrical safety of the equipment, making it more suitable for handling and *in vivo* applications. Of course the shorter discharge duration achieved when the mesh is employed contributes significantly to the reduction of both P_{dis} and i_{RMS} values.

Analyzing the results obtained with glass as the target, it can be seen that both P_{dis} and i_{RMS} curves present similar trends as a function of Q in the wire or mesh configurations. The average P_{dis} values are $\sim 56\%$ higher in the wire configuration when compared to the mesh one, which is almost the same increment as obtained with copper as the target. The i_{RMS} curves differ significantly only for Q values lower than 1.0 l/min, with a small decrement when the wire is used and a small increment in the mesh case, but, in general, the i_{RMS} values are almost the same.

3.2 Spectroscopic emissions and thermal parameters

Figure 5 shows an overview of the emission spectra obtained using Ar as the working gas for the plasma jets produced in the wire and mesh configurations and using the copper target or the glass one. All spectra shown in Fig. 5 exhibit emissions from NO, in the 200 nm to 270 nm wavelength range, OH at 288 nm, 296 nm and 308 nm, with the last two bands jeopardized by N₂ emissions, and from N₂ molecules (N₂ I) in the 298-450 nm range. The hydrogen alpha emission line at 656.28 nm is detected in the spectra obtained using the copper target. Argon line emissions were also observed in all spectra. Regarding the configurations used, there are no significant differences in the emitting species when the remote plasma jet is produced using wire or mesh. The only noticeable difference is the appearance of an ArF molecular emission close to 193 nm when the mesh configuration is employed. That ArF emission was observed previously in an APPJ spectrum by Polak *et al* [11], and its appearance is probably due to the interaction between the Ar plasma jet with the wall of the PTFE tube over which the metal mesh is wrapped.

An important observation to be made about the spectra shown in Fig. 5 is related to the relative intensity of the different emitting species. Although the overall emission intensity with the mesh is low, the relative intensities of OH and NO emissions with respect to N₂ change considerably. The curves for the ratios between the intensity emissions of OH and NO with respect to N₂ (OH/N₂ and NO/N₂, respectively) as a function of Q are shown in Fig. 6. The wavelengths of the emitting species used to calculate the ratios shown in Fig. 6 were 247 nm for NO, 308 nm for OH and 337 nm for N₂.

From Fig. 6(a), it can be seen that for the conducting target the OH/N₂ curves behave differently when the wire or the mesh is used. Regarding the ratio values observed in Fig. 6(a), we see that the OH/N₂ ratio present higher values using the mesh configuration instead the wire one. Furthermore, from Fig. 6(a), we observe that when the APPJ impinges the copper target the mesh configuration tends to provide an optimal OH/N₂ ratio when the gas flow rate is close to 1.5 l/min and that the NO production in relation to N₂ tend to decrease as Q increases.

When the glass target is employed the behavior of OH/N₂ curves shown in Fig. 6(b) present the same trend when wire or mesh configuration are used. A point that is noticeable here is that the OH/N₂ ratio tends to be higher when the mesh configuration is employed. Regarding the NO/N₂ ratio, the behavior of the curves shown in Fig. 6(b) are quite different when the configuration is changed. Being that with the wire configuration the NO/N₂ present a nearly parabolic shape with

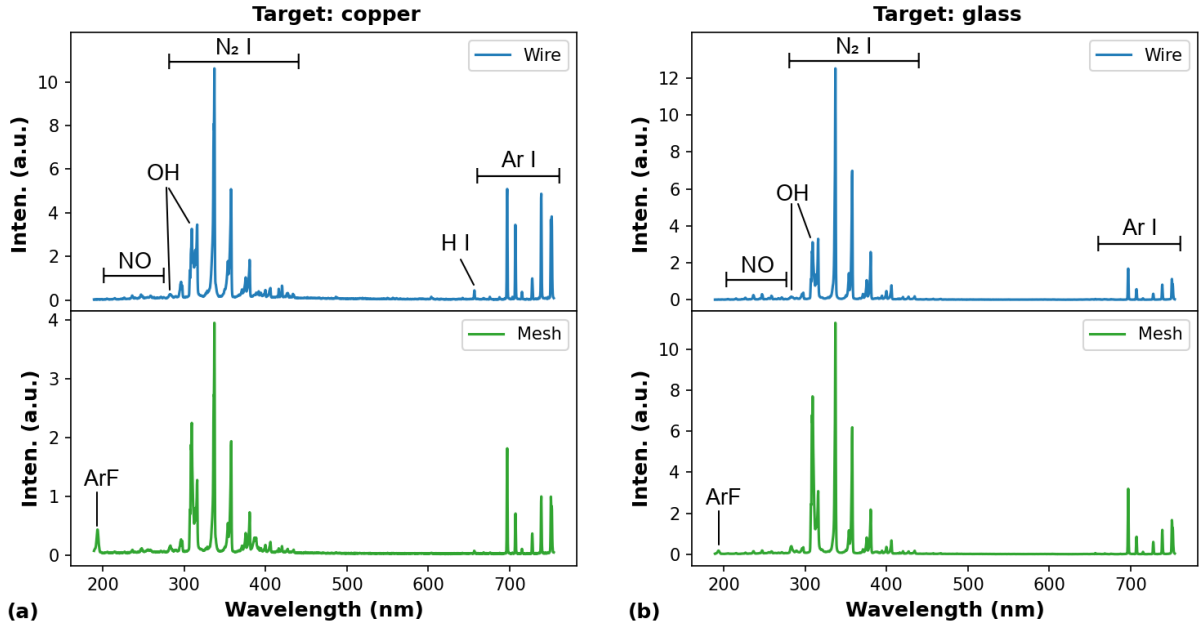


Figure 5: Overview of the emission spectra of the plasma jets obtained for the two different configurations with (a) copper and (b) glass as targets. The gas flow rate was 2.0 l/min in all cases.

a peak value at $Q \approx 2.0$ l/min. On the other hand, the NO/N₂ curve obtained with the mesh mounting decrease monotonically as Q is increased.

It is important to mention that the uncertainty in the intensity measurements are of the order of 1%, and the repeatability of measurements changes no more than 3% under the same environmental conditions. Then, the uncertainties in the intensity ratio calculation are unlikely to cause a significant change in the behavior of the curves shown in Fig. 6.

Regarding the thermal parameters of the APPJs produced using the configurations under study, we measured only the rotational and vibrational temperatures (T_{rot} and T_{vib} , respectively). These two thermal parameters can be considered the main ones for APPJs, since T_{vib} is related to the rate of chemical reactions, and T_{rot} has a close relationship with the gas temperature (T_{gas}), with $T_{rot} \approx T_{gas}$ in most cases [33, 34, 39, 40].

Figure 7 shows the curves of T_{rot} and T_{vib} as a function of Q , obtained using the two different targets, for the wire and mesh configurations. From Fig. 7(a) it can be seen that when the copper plate is used as the target both T_{rot} and T_{vib} values decrease significantly when we switch from the wire to the mesh configuration. Regarding the T_{rot} values, the reduction observed is more than three times for $Q \leq 1.0$ l/min and more than the double for higher Q values. The proportion in the reduction of T_{vib} was of the order of 50% for $Q \leq 1.0$ l/min with the difference becoming smaller for other Q values.

On the other hand, when the APPJ impinges the dielectric target both T_{rot} and T_{vib} values do not differ significantly between the wire and mesh configurations, presenting also the same trend,

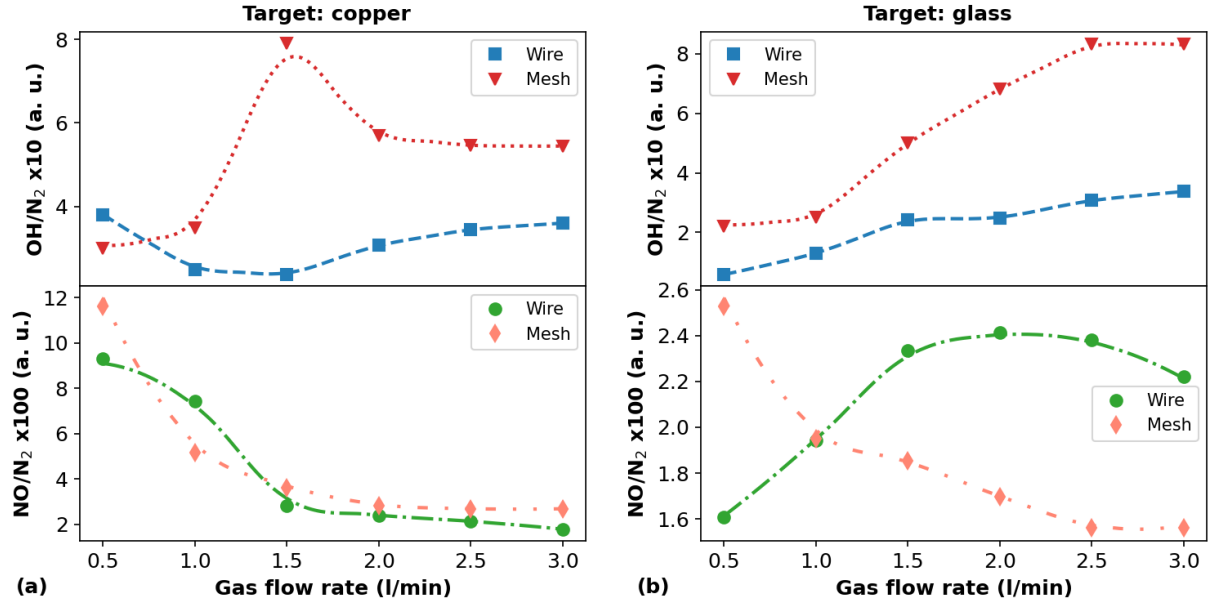


Figure 6: OH/N_2 and NO/N_2 ratios as a function of the gas flow rate for copper (a) and glass (b) targets.

that is, decrease in temperature values as Q is increased. Nevertheless, the T_{vib} values tend to be slightly higher when the wire mounting is employed, and even more for $Q < 1.0 \text{ l/min}$.

It is important to reinforce at this point that the statement $T_{rot} \approx T_{gas}$ is not always valid when the T_{rot} measurements are performed using spectral emissions from the N_2 ($C^3\Pi_u, \nu' \rightarrow B^3\Pi_g, \nu''$) system. This was discussed extensively in a review paper by Bruggeman *et al* [34]. In our work, in particular, the spectroscopy measurements were performed close to the surface of the target and the working gas was argon, which are two conditions in which we have $T_{rot} \neq T_{gas}$, according to [34]. However, we prefer to perform the spectroscopic measurements close to the target surface because this can provide a better insight about the plasma-material interaction. From the T_{rot} curves presented in Fig. 7, it can be seen clearly that the employment of the conducting target leads to T_{rot} values much higher than the dielectric one when the wire configuration is used. This probably happens because the plasma jet tends to enter in a corona regime, which is a plausible hypothesis taking into account that the electrical current also present higher values (see Figs. 3(a) and 4(a)) in this configuration.

In summary, when the APPJ impinges the copper target both T_{rot} and T_{vib} are always smaller for the mesh configuration and tend to not differ significantly when the configuration is changed when the target is the glass plate. Furthermore, the T_{rot} and T_{vib} values obtained in this work are in agreement with others reported in the literature for APPJs that employ Ar as the working gas[41, 42, 43].

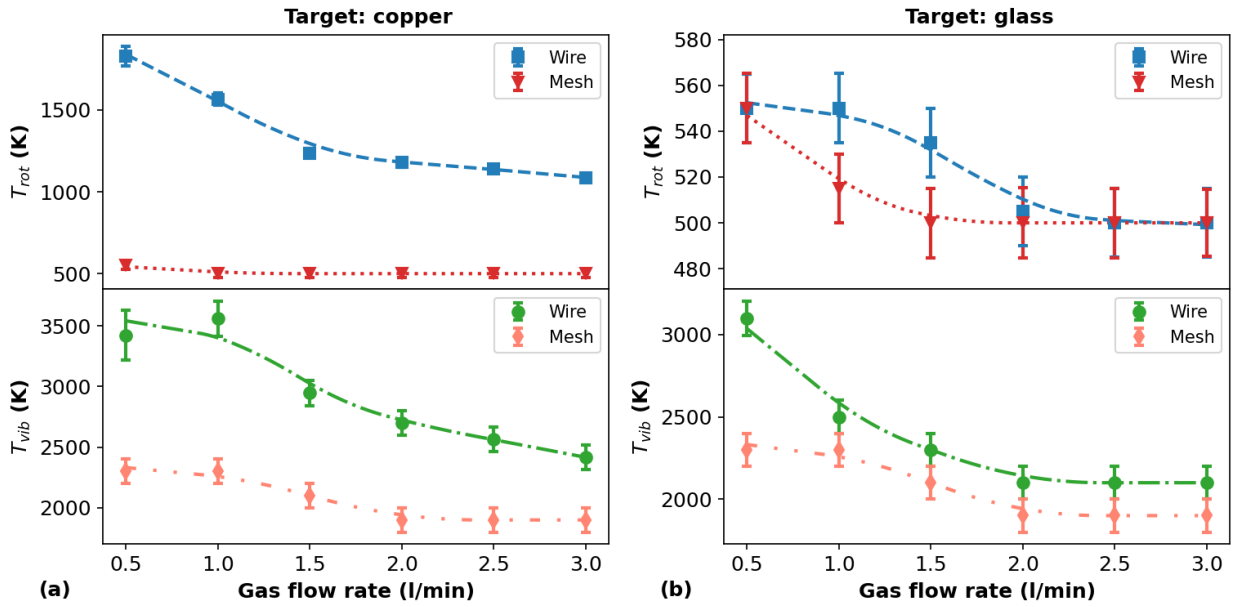


Figure 7: Rotational and vibrational temperatures as a function of the gas flow rate for copper (a) and glass (b) targets.

3.3 Effects on the surface of polymer

The effects of plasma treatment on the surfaces of PP samples using both wire and mesh configurations were evaluated through analysis of the surface morphology, measurements of the water contact angle (WCA) and X-ray photoelectron spectroscopy (XPS) analysis. In all cases, the treated and non-treated samples were compared. In samples that were submitted to APPJ treatment the plasma jet was directed at normal incidence to a position close to their center. In all cases studied in this section, the working gas employed in the plasma treatments was Ar at a flow rate of 2.0 l/min, and the distance between the plasma outlet and the sample was 6 mm in both configurations.

3.3.1 WCA analysis

The effect of the APPJ exposure on the WCA of PP samples was analyzed as a function of treatment time and the results are shown in Fig. 8. From Fig. 8, it is clear that the plasma jet produced with the wire configuration is able to reduce the WCA values faster than the plasma jet obtained with the mesh, and also makes WCA values smaller in the treatment period under analysis.

The behavior of the WCA values as a function of the treatment time is almost the same in both wire and mesh configurations, presenting an abrupt decrease for treatment times up to 20 seconds followed by a slightly increasing plateau. Those increments in the WCA values for exposure times higher than 20 s shown in Fig. 8 suggests that an etching of the functional groups created on the surfaces of the samples during APPJ treatment may be occurring.

The measured values of the discharge power when the plasma jets were applied to PP samples were $P_{dis} = (3.1 \pm 0.2)$ W for the wire configuration and $P_{dis} = (2.7 \pm 0.3)$ W for the mesh one. The

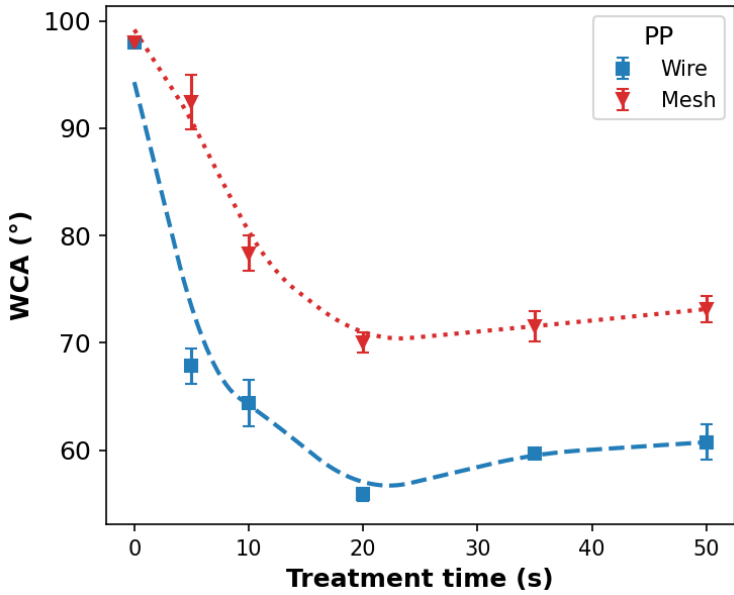


Figure 8: WCA measurements as a function of the APPJ treatment time.

rotational and vibrational temperature values measured when the sample was a dielectric material were $T_{rot} \approx 600$ K and $T_{vib} \approx 2300$ K for wire and $T_{rot} \approx 500$ K and $T_{vib} \approx 1900$ K for mesh. Taking into account that all these parameters have higher values when the wire configuration is employed on the material treatments, one of the explanations for the higher reduction in the WCA values is related to a synergistic effect among such parameters. However, the shorter discharge duration observed when the mesh configuration is employed must also be considered, since this effectively reduces the APPJ exposure time of the material under treatment. From Fig. 8 it can be seen that the WCA values for treatment times equal or greater than 10 s obtained with the mesh mounting is nearly 20% higher than those obtained for the wire case. On the other hand, the discharge duration when using the wire configuration is $\sim 35\%$ higher than the discharge duration of the mesh one, which correlates with the lower WCA values obtained in this case.

3.3.2 XPS analysis of APPJ treated PP samples

The surface chemical composition of the PP samples was investigated by XPS analysis. The obtained results are shown in tables 1 to 3. Table 1 shows of the element fractions detected on the sample surfaces before and after APPJ treatment using the wire and mesh configurations. In both cases were observed reductions in the carbon (C) content on the surfaces which are accompanied by increments in the oxygen (O) content. Small amounts of nitrogen (N) were also detected in the samples after APPJ treatment. When the mesh configuration was employed, traces of fluorine (F) were also detected on the PP surface, probably coming from the PTFE tube due to the plasma-material interaction.

In Table. 2 are shown the element ratios N/C and O/C, in percentage. The O/C ratios make more evident the reduction in the C fraction and the increment in the O fraction shown in Table. 1. The N/C ratios shown in Table. 2 do not change in the same proportion as in the O/C ratios.

Table 1: Averaged elemental composition, in percentage, of PP samples before and after plasma treatment.

	C (%)	O (%)	N (%)
Untreated	98.8	~0.2	~0.9
Wire	80.7 ± 0.9	17.8 ± 0.9	1.4 ± 0.1
Mesh	86.7 ± 0.8	12.3 ± 0.8	0.72 ± 0.06

However, they show clearly that the insertion of N into the PP surfaces is higher when the wire configuration is used.

Table 2: Comparison between average element ratios, in percentage, resulting from APPJ treatments with wire and mesh configurations.

	O/C (%)	N/C (%)
Untreated	~0.91	~0.21
Wire	22.4 ± 1.3	1.8 ± 0.2
Mesh	14.3 ± 1.0	0.84 ± 0.08

Finally, Table. 3 shows the bindings in C 1s peak obtained after APPJ treatment for the components C-C/C-H, C-OH/R, C=O and COOH/R, whose binding energies are 285.0 eV, 286.7 eV, 287.8 eV and 289.2 ± 0.2 eV, respectively. The APPJ treatments performed with both wire and mesh configurations present reductions in the C-C/C-H components and increments in the C-OH/R, C=O and COOH/R ones, as a consequence of the reduction in the C fraction and increment of O fraction, respectively. The XPS results shown in tables 1 to 3 proves the insertion of O-containing functional groups (hydroxyls, carbonyls, carboxyls) on the surface of the PP samples as the O-fraction is increased compared to the non treated PP-material.

Concerning the differences in the amount of functional groups detected on the PP surfaces after APPJ treatment with the different configurations, we can see that the wire mounting provides a higher reduction of the C-C/C-H components and a more efficient insertion of O-containing ones compared to the employment of the mesh mounting.

Table 3: Comparison of average bindings in C 1s peaks, in percentage, resulting from APPJ treatments with wire and mesh configurations.

	C-C/C-H (%)	C-OH (%)	C=O (%)	COOH (%)
Untreated	98.8	~1.2	~0.0	~0.0
Wire	75.6 ± 1.5	9.6 ± 0.5	6.7 ± 0.4	8.0 ± 0.6
Mesh	85.0 ± 1.2	6.5 ± 0.4	3.8 ± 0.3	4.8 ± 0.4

By analyzing the set of results obtained through XPS measurements, we can safely state that the presence of O-containing functional groups, together with the reduction of C-C/C-H ones, on the PP surfaces are the main responsible for the WCA reduction presented in Fig. 8.

3.3.3 Analysis of the surface morphology

In Fig. 9 are shown microphotographs of the morphology of PP samples measured using an optical profiler together with the corresponding RMS roughness (R_q) values obtained before and after plasma treatment. The profilometry performed on the samples shown in Fig. 9 was carried out in an area of $10 \mu\text{m} \times 10 \mu\text{m}$. In addition, profilometry measurements were also performed scanning an area of $200 \mu\text{m} \times 200 \mu\text{m}$. The R_q values obtained for this larger area were $27 \pm 7 \text{ nm}$ for the non treated sample, $29 \pm 6 \text{ nm}$ after treatment using the wire configuration and $33 \pm 10 \text{ nm}$ for the mesh one. By observing the surface profiles and the corresponding R_q value obtained for each sample, it can be seen that the surface morphology is not much affected by APPJ treatment. Concerning the employment of the different configurations on the modification of the surfaces, it can be seen that both wire and mesh configurations tend to generate an increment in the surface roughness.

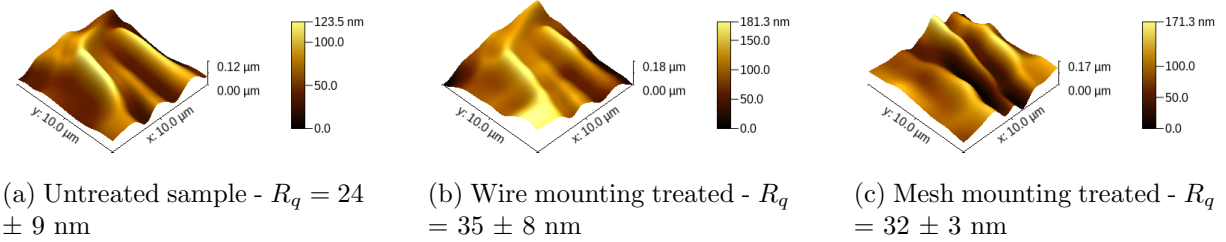


Figure 9: Surface morphologies of PE and PP samples before and after plasma treatment.

From Fig. 9 and from the R_q values obtained for the PP-material it can be inferred that the APPJ treatments do not cause a substantial physical damage on the samples because the surface morphologies do not present drastic changes when comparing the treated and non-treated materials. This is a point that differs from what is found in the literature, since most works have been reported significant changes in the surfaces of the PP material. Usually, APPJ treatments introduce small scale roughness on the material surfaces. [44, 45, 46]. A possible explanation for this difference in relation to what is usually reported in the literature may be related to the higher density of the materials used in this study. This makes the surface hardness be higher, which difficult morphological modifications by APPJ treatment.

4 Conclusions

In this work we report on a different design concept to generate APPJs using long and flexible tubes in an assembly that uses a metallic mesh between two plastic tubes in a concentric arrangement. The plasma jet parameters obtained with this configuration and the application on treatment of polymeric materials were compared to those from a device mounting that employs a long tube with a metal wire inside it. Both arrangements work using the jet transfer technique. Taking into account the P_{dis} values obtained in the wire or the mesh configurations, it is safe to say that the wire one is better for applications which require higher P_{dis} values. However, considering the i_{RMS} values measured in the different configurations, the mesh one would be the most suitable choice for application that require lower electrical current values, like the *in vivo* ones.

Concerning the thermal parameters of the APPJs obtained with the wire and mesh configurations, the T_{rot} values measured with are significantly lower when the mesh mounting is employed and the target is copper. Since T_{rot} has close a relationship with T_{gas} , the use of the mesh mounting seems to be more appropriated for applications in sensitive materials that present significant conductivity.

Regarding the production of reactive species, the relative production of excited OH tends to be higher when the mesh configuration is employed. The relative production of excited NO does not differ significantly when the configuration is changed and the APPJ impinges a metallic target. On the other hand, when the target is a dielectric material, the production of NO species present a tendency to be higher when the wire mounting is employed. Thus, taking into account the differences in the relative production of OH and NO, the choice between wire and mesh configurations must take into account the need for larger amounts of one species or another for the desired application.

The results on the polymer treatment using both configurations have shown that the set of parameters obtained for the plasma jet in the wire configuration lead to better results in terms of WCA reduction and insertion of O-containing functional groups on the surface of the PP material. Also, the WCA and XPS measurements revealed that the APPJ treatment insert O-containing functional groups on the polymer surfaces, which is the main reason for the WCA reduction.

An interesting point regarding the employment of the mesh design is that the mesh itself could be replaced by a metallic film covering the outer wall of the inner tube. This possibility would allow the use of inner tubes with very small diameters, which in turn would provide a very narrow plasma jet that would fit well in dental treatments for example, which require the application of APPJs in very specific and small areas. Of course, this configuration can also be employed in APPJ devices that do not use the jet transfer technique.

In a future work, we intend to investigate the longitudinal distribution of the APPJ treatment on PP and also on other polymer surfaces. Moreover, we intend to perform a detailed study of how a plasma jet propagates in long tubes employing the mesh configuration.

Acknowledgements

The authors thank the Leibniz Institute for Plasma Science and Technology (INP) for the access to the XPS facility and the Center for Semiconducting Components, Nanotechnologies (CCSNano) for providing the surface morphology measurements and the master's student Bruno Silva Leal for cleaning the PP samples used in this work. This research was supported by FAPESP (grants #2019/05856-7 and #2020/09481-5).

References

- [1] Ronny Brandenburg. Dielectric barrier discharges: progress on plasma sources and on the understanding of regimes and single filaments. *Plasma Sources Sci. Technol.*, 26(5):053001, March 2017. Publisher: IOP Publishing.
- [2] Sander Bekeschus, Pietro Favia, Eric Robert, and Thomas von Woedtke. White paper on plasma for medicine and hygiene: Future in plasma health sciences. *Plasma Processes and Polymers*, 16(1):1800033, 2019. eprint: <https://onlinelibrary.wiley.com/doi/pdf/10.1002/ppap.201800033>.

- [3] Giovanni Busco, Eric Robert, Nadira Chettouh-Hammas, Jean-Michel Pouvesle, and Catherine Grillon. The emerging potential of cold atmospheric plasma in skin biology. *Free Radical Biology and Medicine*, 161:290–304, December 2020.
- [4] Dawei Liu, Yanzhe Zhang, Maoyuan Xu, Hongxiang Chen, Xinpei Lu, and Kostya (Ken) Ostrikov. Cold atmospheric pressure plasmas in dermatology: Sources, reactive agents, and therapeutic effects. *Plasma Processes and Polymers*, n/a(n/a):e1900218, February 2020.
- [5] X. Lu, G. V. Naidis, M. Laroussi, S. Reuter, D. B. Graves, and K. Ostrikov. Reactive species in non-equilibrium atmospheric-pressure plasmas: Generation, transport, and biological effects. *Physics Reports*, 630:1–84, May 2016.
- [6] Xiaoqian Cheng, Jonathan Sherman, William Murphy, Edward Ratovitski, Jerome Canady, and Michael Keidar. The Effect of Tuning Cold Plasma Composition on Glioblastoma Cell Viability. *PLOS ONE*, 9(5):e98652, May 2014. Publisher: Public Library of Science.
- [7] Tsung-Wen Chen, Chih-Tung Liu, Chao-Yu Chen, Mu-Chien Wu, Po-Chien Chien, Yun-Chien Cheng, and Jong-Shinn Wu. Analysis of Hydroxyl Radical and Hydrogen Peroxide Generated in Helium-Based Atmospheric-Pressure Plasma Jet and in Different Solutions Treated by Plasma for Bioapplications. *ECS J. Solid State Sci. Technol.*, 9(11):115002, June 2020. Publisher: The Electrochemical Society.
- [8] Dong Ha Kim, Choon-Sang Park, Bhum Jae Shin, Jeong Hyun Seo, and Heung-Sik Tae. Uniform Area Treatment for Surface Modification by Simple Atmospheric Pressure Plasma Treatment Technique. *IEEE Access*, 7:103727–103737, 2019. Conference Name: IEEE Access.
- [9] Thalita M. C. Nishime, Robert Wagner, and Konstantin G. Kostov. Study of Modified Area of Polymer Samples Exposed to a He Atmospheric Pressure Plasma Jet Using Different Treatment Conditions. *Polymers*, 12(5):1028, May 2020. Number: 5 Publisher: Multidisciplinary Digital Publishing Institute.
- [10] Eric Robert, Emerson Barbosa, Sébastien Dozias, Marc Vandamme, Christophe Cachoncinlle, Raymond Viladrosa, and Jean Michel Pouvesle. Experimental Study of a Compact Nanosecond Plasma Gun. *Plasma Processes and Polymers*, 6(12):795–802, 2009. _eprint: <https://onlinelibrary.wiley.com/doi/pdf/10.1002/ppap.200900078>.
- [11] Martin Polak, Jörn Winter, Uta Schnabel, Jörg Ehlbeck, and Klaus-Dieter Weltmann. Innovative Plasma Generation in Flexible Biopsy Channels for Inner-Tube Decontamination and Medical Applications. *Plasma Processes and Polymers*, 9(1):67–76, 2012. _eprint: <https://onlinelibrary.wiley.com/doi/pdf/10.1002/ppap.201000163>.
- [12] Uta Schnabel, Tanja Maucher, Johanna Köhnlein, Wolfram Volkwein, Rijana Niquet, Iris Trick, Manfred Stieber, Michael Müller, Heinz-Peter Werner, Jörg Ehlbeck, Christian Oehr, and Klaus-Dieter Weltmann. Multicentre Trials for Decontamination of Fine-Lumen PTFE Tubes Loaded with Bacterial Endospores by Low and Atmospheric Pressure Plasma. *Plasma Processes and Polymers*, 9(1):37–47, 2012. _eprint: <https://onlinelibrary.wiley.com/doi/pdf/10.1002/ppap.201000206>.

[13] Jiahui Liu, Ruixue Wang, Hongyang Yuan, Wenchao Cai, Xiaoying Wang, Jue Zhang, and Jing Fang. MRI-Guided Dielectric Barrier Discharge Plasma In Vivo: A Preliminary Study for Rectal Wall of Rabbit. *Plasma Processes and Polymers*, 11(12):1188–1192, 2014. _eprint: <https://onlinelibrary.wiley.com/doi/pdf/10.1002/ppap.201400196>.

[14] Mohammed Yousfi, Nofel Merbahi, Atul Pathak, and Olivier Eichwald. Low-temperature plasmas at atmospheric pressure: toward new pharmaceutical treatments in medicine. *Fundamental & Clinical Pharmacology*, 28(2):123–135, April 2014. Publisher: John Wiley & Sons, Ltd.

[15] Konstantin G. Kostov, Munemasa Machida, Vadym Prysiaznyi, and Roberto Y. Honda. Transfer of a cold atmospheric pressure plasma jet through a long flexible plastic tube. *Plasma Sources Sci. Technol.*, 24(2):025038, April 2015. Publisher: IOP Publishing.

[16] Yongdong Liang, Yinglong Li, Ke Sun, Qian Zhang, Wei Li, Weidong Zhu, Jue Zhang, and Jing Fang. Plasma Thorns: Atmospheric Pressure Non-Thermal Plasma Source for Dentistry Applications. *Plasma Processes and Polymers*, 12(10):1069–1074, 2015. _eprint: <https://onlinelibrary.wiley.com/doi/pdf/10.1002/ppap.201400185>.

[17] Aline Chiodi Borges, Gabriela de Moraes Gouvêa Lima, Thalita Mayumi Castaldelli Nishime, Aline Vidal Lacerda Gontijo, Konstantin Georgiev Kostov, and Cristiane Yumi Koga-Ito. Amplitude-modulated cold atmospheric pressure plasma jet for treatment of oral candidiasis: In vivo study. *PLOS ONE*, 13(6):e0199832, June 2018. Publisher: Public Library of Science.

[18] Junxiao Geng, Shaohui Yin, Shuai Huang, Qingchun Tang, Hu Luo, and Fengjun Chen. Flexible cold plasma jet with controllable length and temperature for hydrophilic modification. *Physics of Plasmas*, 25(8):083508, August 2018. Publisher: American Institute of Physics.

[19] Azadeh Valinataj Omran, Alibi Baitukha, Jerome Pulpitel, Farshad Sohbatzadeh, and Farzaneh Arefi-Khonsari. Atmospheric pressure surface modification and cross-linking of UHMWPE film and inside HDPE tube by transporting discharge. *Plasma Processes and Polymers*, 15(1):1700145, 2018. _eprint: <https://onlinelibrary.wiley.com/doi/pdf/10.1002/ppap.201700145>.

[20] Qingchun Tang, Shaohui Yin, Fengjun Chen, Shuai Huang, and Hu Luo. New technology for cutting ferrous metal with diamond tools. *Diamond and Related Materials*, 88:32–42, September 2018.

[21] Jörn Winter, Thalita M.C. Nishime, Sven Glitsch, Heike Lühder, and Klaus-Dieter Weltmann. On the development of a deployable cold plasma endoscope. *Contributions to Plasma Physics*, 58(5):404–414, 2018. _eprint: <https://onlinelibrary.wiley.com/doi/pdf/10.1002/ctpp.201700127>.

[22] Manabu Kurosawa, Toshihiro Takamatsu, Hiroaki Kawano, Yuta Hayashi, Hidekazu Miyahara, Syosaku Ota, Akitoshi Okino, and Masaru Yoshida. Endoscopic Hemostasis in Porcine Gastrointestinal Tract Using CO₂ Low-Temperature Plasma Jet. *Journal of Surgical Research*, 234:334–342, February 2019. Publisher: Elsevier.

[23] Irina Schweigert, Dmitry Zakrevsky, Pavel Gugin, Elena Yelak, Ekaterina Golubitskaya, Olga Troitskaya, and Olga Koval. Interaction of Cold Atmospheric Argon and Helium Plasma Jets with Bio-Target with Grounded Substrate Beneath. *Applied Sciences*, 9(21):4528, January 2019. Number: 21 Publisher: Multidisciplinary Digital Publishing Institute.

[24] Orianne Bastin, Max Thulliez, Jean Servais, Antoine Nonclercq, Alain Delchambre, Alia Hadefi, Jacques Devière, and François Reniers. Optical and Electrical Characteristics of an Endoscopic DBD Plasma Jet. *PMED*, 10(2), 2020. Publisher: Begel House Inc.

[25] Yun-Hsuan Chen, Jang-Hsing Hsieh, I.-Te Wang, Pei-Ru Jheng, Yi-Yen Yeh, Jyh-Wei Lee, Nima Bolouki, and Er-Yuan Chuang. Transferred Cold Atmospheric Plasma Treatment on Melanoma Skin Cancer Cells with/without Catalase Enzyme In Vitro. *Applied Sciences*, 11(13):6181, January 2021. Number: 13 Publisher: Multidisciplinary Digital Publishing Institute.

[26] Zhongmin Xiong, Eric Robert, Vanessa Sarron, Jean-Michel Pouvesle, and Mark J. Kushner. Atmospheric-pressure plasma transfer across dielectric channels and tubes. *J. Phys. D: Appl. Phys.*, 46(15):155203, March 2013. Publisher: IOP Publishing.

[27] Yang Xia, Dongping Liu, Wenchun Wang, Yifeng Peng, Jinhai Niu, Zhenhua Bi, Longfei Ji, Ying Song, Xueyang Wang, and Zhihua Qi. The transfer of atmospheric-pressure ionization waves via a metal wire. *Physics of Plasmas*, 23(1):013509, January 2016. Publisher: American Institute of Physics.

[28] Jörn Winter, Thalita M. C. Nishime, Robert Bansemer, Martina Balazinski, Kristian Wende, and Klaus-Dieter Weltmann. Enhanced atmospheric pressure plasma jet setup for endoscopic applications. *J. Phys. D: Appl. Phys.*, 52(2):024005, November 2018. Publisher: IOP Publishing.

[29] Iu Onyshchenko, Nathalie De Geyter, Anton Yu Nikiforov, and Rino Morent. Atmospheric Pressure Plasma Penetration inside Flexible Polymeric Tubes. *Plasma Processes and Polymers*, 12(3):271–284, March 2015. Publisher: John Wiley & Sons, Ltd.

[30] Marcin Hołub. On the measurement of plasma power in atmospheric pressure DBD plasma reactors. *International Journal of Applied Electromagnetics and Mechanics*, 39(1-4):81–87, January 2012. Publisher: IOS Press.

[31] David E. Ashpis, Matthew C. Laun, and Elmer L. Griebeler. Progress Toward Accurate Measurement of Dielectric Barrier Discharge Plasma Actuator Power. *AIAA Journal*, 55(7):2254–2268, 2017.

[32] Andrei V. Pipa and Ronny Brandenburg. The Equivalent Circuit Approach for the Electrical Diagnostics of Dielectric Barrier Discharges: The Classical Theory and Recent Developments. *Atoms*, 7(1):14, March 2019. Number: 1 Publisher: Multidisciplinary Digital Publishing Institute.

[33] Se Youn Moon and W. Choe. A comparative study of rotational temperatures using diatomic OH, O₂ and N₂⁺ molecular spectra emitted from atmospheric plasmas. *Spectrochimica Acta Part B: Atomic Spectroscopy*, 58(2):249–257, February 2003.

[34] P. J. Bruggeman, N. Sadeghi, D. C. Schram, and V. Linss. Gas temperature determination from rotational lines in non-equilibrium plasmas: a review. *Plasma Sources Sci. Technol.*, 23(2):023001, April 2014.

[35] Q. Y. Zhang, D. Q. Shi, W. Xu, C. Y. Miao, C. Y. Ma, C. S. Ren, C. Zhang, and Z. Yi. Determination of vibrational and rotational temperatures in highly constricted nitrogen plasmas by fitting the second positive system of N₂ molecules. *AIP Advances*, 5(5):057158, May 2015. Publisher: American Institute of Physics.

[36] Ryo Ono. Optical diagnostics of reactive species in atmospheric-pressure nonthermal plasma. *J. Phys. D: Appl. Phys.*, 49(8):083001, January 2016. Publisher: IOP Publishing.

[37] Jan Voráč, Petr Synek, Lucia Potočnáková, Jaroslav Hnilica, and Vít Kudrle. Batch processing of overlapping molecular spectra as a tool for spatio-temporal diagnostics of power modulated microwave plasma jet. *Plasma Sources Sci. Technol.*, 26(2):025010, January 2017. Publisher: IOP Publishing.

[38] Jan Voráč, Petr Synek, Vojtěch Procházka, and Tomáš Hoder. State-by-state emission spectra fitting for non-equilibrium plasmas: OH spectra of surface barrier discharge at argon/water interface. *J. Phys. D: Appl. Phys.*, 50(29):294002, June 2017. Publisher: IOP Publishing.

[39] J. D. Lambert. Vibration–vibration energy transfer in gaseous collisions. *Q. Rev. Chem. Soc.*, 21(1):67–78, January 1967.

[40] R. R. Smith, D. R. Killelea, D. F. DelSesto, and A. L. Utz. Preference for Vibrational over Translational Energy in a Gas-Surface Reaction. *Science*, 304(5673):992–995, May 2004.

[41] M. Bazavan, M. Teodorescu, and G. Dinescu. Confirmation of OH as good thermometric species for gas temperature determination in an atmospheric pressure argon plasma jet. *Plasma Sources Sci. Technol.*, 26(7):075001, June 2017. Publisher: IOP Publishing.

[42] Jing Li, Bingying Lei, Jing Wang, Tongyi Zhang, Jie Tang, Yishan Wang, Wei Zhao, and Yixiang Duan. A Filamentary Plasma Jet Generated by Argon Dielectric-Barrier Discharge in Ambient Air. *IEEE Transactions on Plasma Science*, 47(7):3134–3140, July 2019. Conference Name: IEEE Transactions on Plasma Science.

[43] Jie Yu, Wencong Zhang, Xiao Wu, Li Wu, Junwu Tao, and Kama Huang. The influence of gas humidity on the discharge properties of a microwave atmospheric-pressure coaxial plasma jet. *AIP Advances*, 11(2):025131, February 2021. Publisher: American Institute of Physics.

[44] K. G. Kostov, T. M. C. Nishime, A. H. R. Castro, A. Toth, and L. R. O. Hein. Surface modification of polymeric materials by cold atmospheric plasma jet. *Applied Surface Science*, 314:367–375, September 2014.

[45] Matic Resnik, Janez Kovač, Roman Štukelj, Veronika Kralj-Iglič, Petr Humpolíček, and Ita Junkar. Extracellular Vesicle Isolation Yields Increased by Low-Temperature Gaseous Plasma Treatment of Polypropylene Tubes. *Polymers*, 12(10):2363, October 2020. Number: 10 Publisher: Multidisciplinary Digital Publishing Institute.

[46] J. Turicek, N. Ratts, M. Kaltchev, and N. Masoud. Investigation of a helium tubular cold atmospheric pressure plasma source and polymer surface treatment application. *Plasma Sources Sci. Technol.*, 30(2):025005, February 2021. Publisher: IOP Publishing.